

RESEARCH

Open Access



Hydrogen, helium and thermo-acoustic refrigerators

B. G. Prashantha^{1*}, G. S. V. L. Narasimham², S. Seetharamu³ and Vinayak B. Hemadri⁴

Abstract

In this work the design and analysis of 1 kW thermo-acoustic refrigerators with hydrogen and helium for the temperature difference of 38 K is discussed. Helium is the best for thermoacoustic refrigerators compared to the other competent gases. But hydrogen is chosen since it is less expensive and better thermophysical properties compared to helium. The best parallel plates geometry with 15% blockage is chosen for the stack and heat exchangers. The effect of resonance frequency of hydrogen and helium varying from 400–600 Hz on the theoretical performance is discussed. The coefficient of performance and the power density of 1.65 and 40.3 kW/m³ for hydrogen, and 1.58 and 19.2 kW/m³ for helium is reported for the optimized designs, respectively. The theoretical results are compared with the DeltaEC software results, shows the cooling power and coefficient of performance of 590 W and 1.11 for hydrogen, and 687 W and 1.25 for helium, respectively.

Keywords Parallel plate stack-heat exchangers, TDH resonator, DeltaEC

1 Introduction and review of literature

The stack-based standing wave thermoacoustic refrigerators are the low cost, eco-friendly and promising technology and which can be built indigenously with only moving component as magnetic coil for room temperature refrigeration. The thermoacoustic coolers are expected to replace the existing vapour compressor refrigeration systems for household and commercial applications. In the recent years, thermoacoustic cooling receives the attentions of the researchers worldwide to optimize the coolers both theoretically and practically, ranging from 3–500 W at a reasonable and promising coefficient of performance of 0.5–1.8 [1–4]. Thermoacoustic coolers may be

driven by thermoacoustic engine or loudspeaker. The loudspeaker that drives the thermoacoustic cooler is the simple and readily available in the commercial market, and which can be modified easily to improve efficiency compared to the thermoacoustic engines [5–7]. The pictorial representation of the thermo-acoustic refrigerator powered by commercial loudspeaker is depicted in Fig. 1. The commercial loudspeaker firmly fixed with the duct left to the ambient heat exchanger, followed by the parallel plate stack and cold heat-exchanger. The taper section fastened right to the cold heat-exchanger. The compact quarter wave length divergent-hemispherical resonator fastened to the taper section (Fig. 1) is the efficient design over the small diameter tube design as discussed elsewhere [3, 4, 8].

The loudspeaker supplies acoustic energy because of its vibrating diaphragm to the filled in gas of a resonator. Upon electrical energy to the loudspeaker, the gas starts oscillating through the porous stack-heat-exchangers, the taper and the divergent section. The methodology of choosing the geometrical specifications and the positions of the stack, heat-exchangers, resonator and the loudspeaker of the cooler is found elsewhere [9–11]. The gas

*Correspondence:

B. G. Prashantha
bgpsandur@gmail.com

¹ Department of Mechanical Engineering, JSS Academy of Technical Education, Dr. Vishnuvardhan Road, Bengaluru 560 060, India

² Department of Mechanical Engineering, Indian Institute of Science, Bengaluru 560 012, India

³ Formerly Central Power Research Institute, Bengaluru 560 080, India

⁴ Department of Mechanical Engineering, Dayananda Sagar University, Hosur Road, Bengaluru 560 068, India



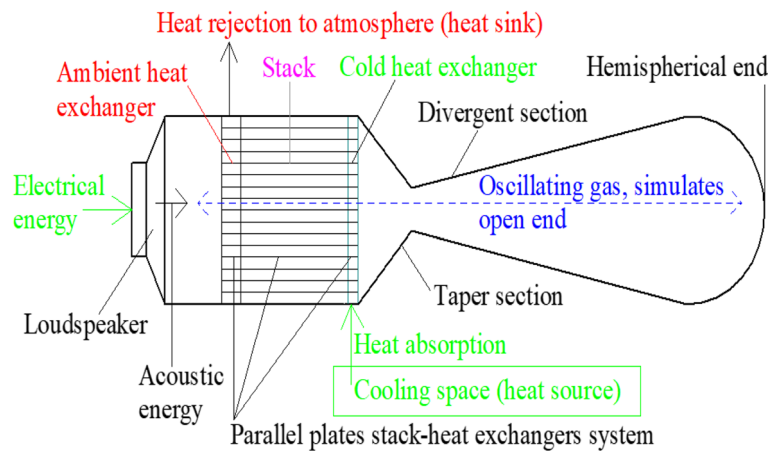


Fig. 1 The pictorial representation showing the thermo-acoustic refrigerator powered by commercial loudspeaker

experiences maximum compression in the ambient heat-exchanger region and maximum rarefaction (expansion) in the cold heat exchanger region during the front and back motion of the coil, respectively. The oscillating gas is considered as the adiabatic parcel since the whole outer surface of the device is assumed to be insulated perfectly with no heat leak losses.

The four thermodynamic processes (Fig. 2) similar to the Bell Coleman’s air refrigeration cycle (reverse Brayton or Joule cycle) are: the process (1–2) and (3–4) represents adiabatic gas compression and expansion, respectively and (4–1) and (2–3) represents isobaric heat absorption and rejection, respectively. The $P-v$, $T-s$ and $P-h$ thermodynamic diagrams with the variation in the temperature, enthalpy and size of the oscillating gas parcel is given in Fig. 2. The gas oscillations gradually decrease the gas temperature in the cold heat-exchanger region, absorbing heat of the cold heat-exchanger plates connected to cooling space. Contrary the gas temperature increases in the ambient heat-exchanger region, reject heat to the atmosphere via the ambient heat-exchanger plates at room temperature using the water-cooling system [1, 3].

Likewise, the compression and expansion of gas caused by the loudspeaker creates difference in temperature across the ambient and cold heat-exchangers through the stack for heat pumping from the cooling space to the surrounding environment (Fig. 1). In the literature it is found that the working gases for the thermoacoustic refrigerators is chosen based on the better thermophysical properties (high sound velocity and thermal conductivity) and low cost [1, 10]. And the other criterion for the selection of the best gas is the Prandtl number (σ), is the ratio of viscous to thermal diffusion. From the literature [12] it is found that the cooler performance increases with decrease in the Prandtl number of the oscillating gas. Hence the pure or the gas mixture with low Prandtl number is the best for the thermoacoustic coolers. Prandtl number is proportional to dynamic viscosity (μ) and isobaric specific heat (C_p) and varies inversely with thermal conductivity (k) of the oscillating gas. In this research work hydrogen and helium is chosen since both the gases meets the required conditions as the working gases (Table 1). The hydrogen has the higher isobaric specific heat, leading to the marginal increase in the Prandtl

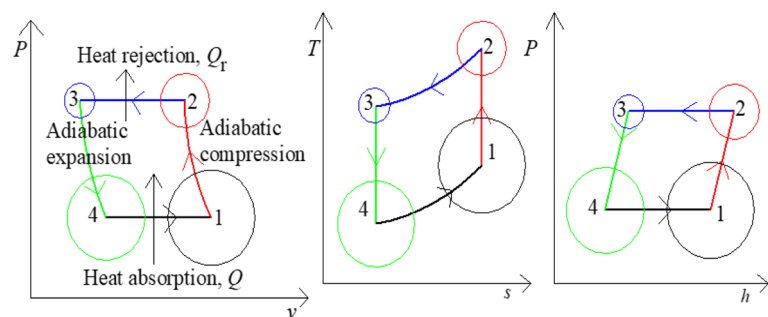


Fig. 2 The $P-v$, $T-s$, and $P-h$ diagrams of a thermo-acoustic cooler with circles around the state points representing the size of a gas parcel undergoing thermodynamic process

Table 1 Thermo-physical properties of hydrogen and helium at 10 bar and 283 K

Gas	γ	u (ms^{-1})	ρ (kgm^{-3})	C_p ($\text{Jkg}^{-1} \text{K}^{-1}$)	k ($\text{Wm}^{-1} \text{K}^{-1}$)	σ	μ ($\text{kgm}^{-1} \text{s}^{-1}$)
H ₂	1.4000	1278	0.8568	14,286	0.1752	0.7024	8.6152E-6
He	1.6667	990	1.7011	5193	0.1508	0.6619	1.9217E-5

number compared to the helium. In this research work the thermoacoustic cooler with 1 kW capacity is theoretically optimized with hydrogen and helium using the parallel plates stack and heat exchangers system. Therefore, the primary objective is to study the effect of resonance frequency of hydrogen and helium operating from 400–600 Hz on the theoretical performance of the cooler is discussed.

The resonance frequency for both the gases is decided based on their better cooling capacity (Q), performance (COP) and power-density of the cooler for the compact design. Hydrogen is cheaper compared to helium and hence an attempt is made to use hydrogen as the competent working gas over helium for the possibility to decrease the cost of the coolers towards commercialization. But the hydrogen is highly inflammable and with proper safety measures the use of hydrogen in thermoacoustic coolers is justifiable. The second objective is to study the effect of increasing the length of the cold heat-exchanger (l_4) from two times the gas displacement ($2x_1$) to four times ($4x_1$) on the theoretical performance is discussed in Sects. 2 and 3. In this research work the length of the cold heat-exchanger equal to four times the gas displacement ($l_4=4x_1$) is considered to avoid the space constraints associated in mounting the thermocouples with the small length at two times the gas displacement ($l_4=2x_1$) as discussed elsewhere [3]. The theoretically

optimized design results with hydrogen and helium are validated with the DeltaEC software simulation results [13], and the conclusions are drawn by considering the design assumptions and limitations.

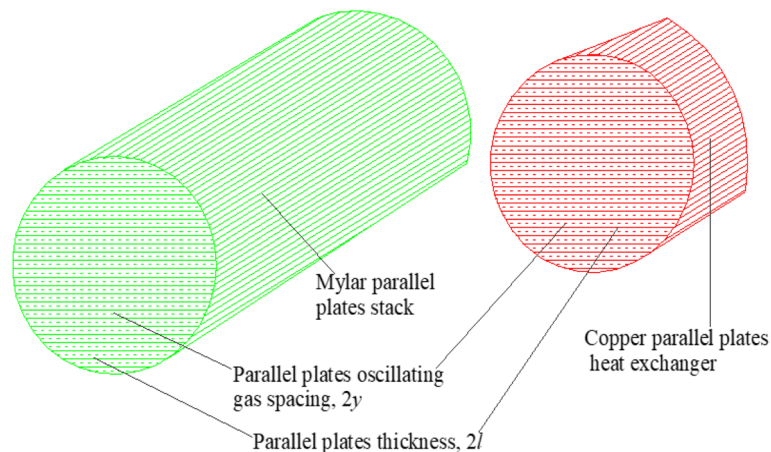
2 Design and analysis of parallel plates stack and heat-exchangers

The design and analysis of the parallel plates stack and heat-exchangers system at 85% porosity ' ϵ ' is discussed. The cross-sectional geometry for the parallel plates stack, cold and ambient heat-exchangers are the same but the length varies. The porosity represents the percentage of the cross-sectional area of the stack and heat-exchangers open for the gas to oscillate. In other words, it is also called as the blockage ratio ' B ', represents the percentage of the solid area offers blockage for the gas to oscillate along its length. The porosity and blockage ratio are given by

$$\epsilon = y \div (y + l) = 85\% \quad (1)$$

$$B = l \div (y + l) = 1 - \epsilon = 15\% \quad (2)$$

where ' l ' and ' y ' are referred to the parallel plates half-thickness and spacing, respectively of the stack-heat exchangers system (Fig. 3). The stack is usually made of mylar material, whereas the cold and ambient

**Fig. 3** A pictorial view of the parallel plates stack and heat exchanger

heat-exchangers is of copper, both made precisely using the popular 3D printing technology. The thermophysical properties of the mylar stack and copper parallel plates at the mean gas temperature $T_{\text{mg}} = 283 \text{ K}$ are: $k_s = 0.158 \text{ Wm}^{-1} \text{ K}^{-1}$, $\rho_s = 1350.5 \text{ kgm}^{-3}$ and $C_{ps} = 1047.1 \text{ Jkg}^{-1} \text{ K}^{-1}$ for the stack; and $k_c = 398.96 \text{ Wm}^{-1} \text{ K}^{-1}$, $\rho_c = 9000 \text{ kgm}^{-3}$ and $C_{pc} = 420 \text{ Jkg}^{-1} \text{ K}^{-1}$ for the cold and ambient heat-exchangers. The 1 kW cooler design is optimized with hydrogen and helium for the temperature difference (θ) of 38 K, assuming the ambient heat-exchanger temperature (T_{ax}) at 301 K using the circulating cooling water system as found in the published literature [2, 3]. The cooler is operating with 10 bar pressure at 3% drive ratio 'D' is the ratio of dynamic pressure amplitude of oscillating gas ' P_a ' to gas pressure ' P '.

In the literature, it is found that the drive ratio should be less than or equal to 3% to avoid the acoustic non-linearities of the system [14]. The viscous penetration depth ' δ_v ' and the thermal penetration depths ' δ_k ' of the oscillating hydrogen and helium are the very thin layers around the parallel plates stack, are given by [9]

$$\delta_v = \sqrt{\frac{2\mu}{\rho(2\pi f)}} \quad (3)$$

$$\delta_k = \sqrt{\frac{2k}{\rho C_p(2\pi f)}} \quad (4)$$

The oscillating gas should have comparatively a lower value of ' δ_v ' which resist the gas movement compared to ' δ_k ' through which the thermo-acoustic heat pumping occurs. The design parameters and the variation

in the values of the penetration depths (' δ_v ' and ' δ_k ') of the hydrogen and helium versus the resonance frequency ' f ' are given in Table 2. The penetration depths are inversely proportional to the resonance frequency of the oscillating gas.

The amplitude of velocity and pressure of the oscillating gas measured at a point ' x ' away from the speaker surface is given by [5]

$$u_1 = \frac{P_a \sin(cx)}{\varepsilon \rho u} \quad (5)$$

$$p_1 = P_a \cos(cx) \quad (6)$$

The gas parcel excursion (displacement amplitude, x_1) is expressed as [5]

$$x_1 = \frac{u_1}{\omega} = \frac{P_a \sin(cx)}{\varepsilon \rho u(2\pi f)} \quad (7)$$

where ' u_1 ' and ' ω ' are the amplitude of gas velocity and angular velocity at a particular location, respectively. For a typical engine or refrigerator, the penetration depths are smaller than the oscillating gas parcel excursion x_1 is given by [15]

$$\delta_v, \delta_k \ll x_1 \quad (8)$$

From the literature it is found that to minimize the altering of the acoustic standing wave in the stack and heat exchangers system, it is recommended to use the parallel plates oscillating gas spacing ($2y$) of $2\delta_k$ to $4\delta_k$ [16–18]. Hence it is chosen to use a gas spacing of $4\delta_k$ to avoid the acoustic disturbances. The stack and heat exchangers plates thickness ($2l$) at 85% porosity is calculated using Eq. (1). The stack and heat-exchangers plates spacing ($2y$) and thickness ($2l$) varies inversely with the resonance frequency for both hydrogen and helium as given in Table 3. The derived parameters, namely the angular velocity (ω), wave number (c), and wavelength (λ) of the hydrogen and helium versus the resonance frequency are presented in Table 4. For the stack-based thermoacoustic cooler or engine, the

Table 2 Effect of resonance frequency on penetration depths

Design parameters	Viscous and thermal penetration depths
Design requirements: $Q = 1 \text{ kW}$, $\theta = 38 \text{ K}$	H₂: f @400 Hz: $\delta_v = 90 \mu\text{m}$, $\delta_k = 107 \mu\text{m}$ f @500 Hz: $\delta_v = 80 \mu\text{m}$, $\delta_k = 96 \mu\text{m}$
Operating parameters: $P = 10 \text{ bar}$, $P_a = 0.3 \text{ bar}$, $T_{\text{mg}} = 283 \text{ K}$, $T_{\text{ax}} = 301 \text{ K}$	He: f @400 Hz: $\delta_v = 73 \mu\text{m}$, $\delta_k = 87 \mu\text{m}$ f @500 Hz: $\delta_v = 95 \mu\text{m}$, $\delta_k = 115 \mu\text{m}$ f @600 Hz: $\delta_v = 85 \mu\text{m}$, $\delta_k = 103 \mu\text{m}$ f @600 Hz: $\delta_v = 77 \mu\text{m}$, $\delta_k = 94 \mu\text{m}$

Table 3 Stack-heat exchangers plate spacing and thickness versus working gas and resonance frequency

Gas @ $2y = 4\delta_k$	f (Hz)		500		600	
	2y (μm)	2l (μm)	2y (μm)	2l (μm)	2y (μm)	2l (μm)
H ₂	428	76	384	68	348	61
He	460	81	412	73	376	66

Table 4 Derived parameters used in the design process

Derived parameters	f (Hz)					
	400		500		600	
	H ₂	He	H ₂	He	H ₂	He
$\omega = 2\pi f$ (rads ⁻¹)	2513	2513	3142	3142	3770	3770
$c = \omega/u$ (m ⁻¹)	1.96	2.54	2.45	3.17	2.94	3.81
$\lambda = u/f$ (m)	3.21	2.48	2.57	1.98	2.14	1.65

parameter which determines the cooler performance is the stack critical temperature (θ_{cr}).

It is the state of the thermo-acoustic stack at which the stack does not pump heat with no temperature difference (θ) exist, is given by [15]

$$\theta_{cr} = \frac{(\gamma - 1)\varepsilon T_{mg}(c.l_3)}{\tan(c.X)} \quad (9)$$

The design parameters are normalized to the 11 dimensionless parameters to simplify the design process and the effect of resonance frequency on the normalized parameters for hydrogen and helium are given in Table 5. If $\theta < \theta_{cr}$ then the normalized critical temperature 'T' (ratio of temperature difference to critical temperature) will be less than one and is true for both hydrogen and helium (Table 5). At this condition the stack plates transfer heat from the cold heat-exchanger to the ambient heat-exchanger to produce refrigeration effect in the cooling space upon the acoustic power input by the loudspeaker (Fig. 1) [19, 20]. The hydrogen has the lower value of the normalized critical temperature (0.4) compared to helium (0.5). Hence the hydrogen cooler can produce better refrigeration effect compared to helium at

the required temperature difference (θ) of 38 K (Table 2). The normalized stack-length ' l_{3n} ' and centre-position ' X_n ' values are optimized between the stack diameter (d_1) and the stack coefficient of performance (COP_s). They are chosen based on the balance between ' d_1 ' and ' COP_s '. The thermal conductivity ' K ' of the parallel plates mylar stack affects its performance because of the reverse conduction of heat from the ambient to cold heat-exchanger and decreases the ' COP_s ' as discussed elsewhere [1, 6, 21].

The normalized cooling-power ' Q_n ' and acoustic-power ' W_n ' equations are derived by considering the heat-capacity ratio and the thermal conductivity of both the gas and the stack using the Rott's thermoacoustic theory is given by [9, 22, 23]

$$Q_n = \frac{-\delta_{kn} D^2 \sin(2X_n)}{8\gamma(1 + \varepsilon_s)(1 + \sigma)\Lambda} \times \left[\Gamma \frac{1 + \sqrt{\sigma} + \sigma}{1 + \sqrt{\sigma}} - (1 + \sqrt{\sigma} - \sqrt{\sigma}\delta_{kn}) \right] - \Lambda^1 \quad (10)$$

$$W_n = \frac{-\delta_{kn} l_{3n} D^2}{4\gamma} \left[\frac{(\gamma - 1)\varepsilon \cos^2(X_n)}{(1 + \varepsilon_s)} \left(\frac{\Gamma}{(1 + \sqrt{\sigma})\Lambda} - 1 \right) - \frac{\sqrt{\sigma} \sin^2(X_n)}{\varepsilon \Lambda} \right] \quad (11)$$

where ε_s , Λ and Λ^1 in Eqs. (10) and (11) are defined as the dimensionless stack heat capacity correction factor, and

Table 5 Effect of the resonance frequency on Dimensionless (Normalized) design parameters optimized for hydrogen and helium

Normalized parameters	f (Hz)					
	400		500		600	
	H ₂	He	H ₂	He	H ₂	He
$\theta/\theta_{cr} = \Gamma$	0.4	0.5	0.4	0.5	0.4	0.5
$\theta/T_{mg} = \theta_n$	0.1343		0.1343		0.1343	
$\delta_k/\gamma = \delta_{kn}$	0.5		0.5		0.5	
$\delta_v/\gamma = \delta_{vn}$	0.421	0.413	0.417	0.413	0.420	0.410
$c.l_3 = l_{3n}$	0.2	0.1	0.2	0.1	0.2	0.1
$c.X = X_n$	0.2	0.2	0.2	0.2	0.2	0.2
$Q/(P u A_1) = Q_n$	1.03E-5	7.10E-6	1.02E-5	6.83E-6	1.01E-5	6.57E-6
$W_s/(P u A_1) = W_n$	4.15E-6	2.58E-6	4.15E-6	2.58E-6	4.15E-6	2.58E-6
$c.l_4 = l_{4n} = l_{2n}$	2.82E-2	2.10E-2	2.82E-2	2.10E-2	2.82E-2	2.10E-2
$c.X_4 = X_{4n}$	3.14E-1	2.60E-1	3.14E-1	2.60E-1	3.14E-1	2.60E-1
$c.X_2 = X_{2n}$	8.59E-2	1.40E-1	8.59E-2	1.40E-1	8.59E-2	1.40E-1

the gas and the stack heat conduction correction factors, respectively, are given by

$$\varepsilon_s = \sqrt{\frac{\rho_g \cdot c_{pg} \cdot k_g}{\rho_s \cdot c_{ps} \cdot k_s}} \quad (12)$$

$$\Lambda = 1 - \delta_{vn} + 0.5\delta_{vn}^2 \quad (13)$$

$$\Lambda^1 = \frac{T_{mg} \cdot c}{P \cdot u \cdot l_{3n}} (\varepsilon k_g + (1 - \varepsilon) k_s) \quad (14)$$

Using the data given in Tables 1, 2, 3 and 4 in Eqs. (10) - (11), the ' Q_n ' and ' W_n ' for the optimized parallel plates stack are determined and presented in Table 5. The coefficient of performance of the stack ' COP_s ' is given by

$$COP_s = \frac{Q_n}{W_n} \quad (15)$$

The stack performance versus the resonance frequency for hydrogen and helium is calculated using Eq. (15) (Table 6). The performance of the stack varies inversely with the resonance frequency because of the increase in the fluid turbulence at higher frequency. The hydrogen has lower performance of the stack compared to helium since the hydrogen has the larger stack length (l_3) which absorb more acoustic power (W_s), leading to decrease in the ' COP_s '. Using the data given in Tables 1, 2 and 5 in the equation $Q_n = Q/(PuA_1)$, the variation of the stack diameter ' d_1 ' versus the resonance frequency ' f ' is determined (Table 6). The ' d_1 ' is proportional to ' f ' for both the hydrogen and helium. This is because the increase in the resonance frequency increases the gas turbulence which decreases the thermal penetration depth (Table 2) and hence the stack diameter increases with increase in the resonance frequency (Table 6). Using the normalized equations and the optimized values given in Table 5, the stack-length (l_3) and the stack-centre point (X) are determined. By using Eq. (7), the oscillating gas displacement amplitude (x_1) at the right-side to the cold end of the

parallel plates stack is determined. The length of the cold heat-exchanger (l_4) at the cold-side of the stack equal to the length $2x_1$ and $4x_1$ is determined (Table 6).

The cold heat-exchanger length equal to the ambient heat-exchanger is taken as: $l_4 = 4x_1 = l_2$ (Table 6). Further, the length between the speaker and the ambient heat-exchanger ' l_1 ' is determined. Using the stack normalized acoustic-power equation $W_s/(PuA_1) = W_n$ and substituting the known values, the acoustic-power dissipation in to the stack ' W_s ' is determined. Similarly, the acoustic-power dissipation in the cold heat-exchanger ' W_{cx} ' and the ambient heat-exchanger ' W_{ax} ' are determined using Eq. (11) by setting the normalized critical temperature (Γ) equal to zero. The values of the normalized equations l_{4n} , X_{4n} , l_{2n} and X_{2n} versus the resonance frequency are determined (Table 5). The frequency of 600 Hz for hydrogen and 400 Hz for helium are chosen to be optimum by considering the balance between the optimized design and performance parameters values, namely the COP_s , d_1 , W_s , W_{cx} , and W_{ax} as given in Table 6.

3 Design and analysis of divergent resonator

The quarter wave-length divergent hollow resonator is a rigid structure made of thin stainless-steel sheets. It connects the loudspeaker and the stack and heat exchangers system and the right-side geometry is the taper-divergent-hemispherical (TDH) design (Fig. 1). The compact TDH design is chosen over the other geometries because of its lower acoustic dissipation losses and improved cooler power-density as discussed in the published literature [1, 24, 25]. The taper length ($L_2 = 20$ mm), the diameter ratio ($d_r = 0.15$) and the hemispherical radius ($r_h = 0.5d_1$) are chosen for the final shape for both hydrogen and helium (Fig. 4). At this geometry of the resonator the acoustic power dissipation losses are minimal and which improves cooling power, coefficient of performance and power-density of the cooler as discussed elsewhere [4, 8]. The divergent section of the resonator is the buffer volume terminated with the hemispherical design (Fig. 4), simulates

Table 6 The optimized specifications and performance parameters of the parallel plates stack and heat exchangers system at $2\gamma = 4\delta_k$ versus working gas and frequency

Gas	f (Hz)	l_3 (mm)	X (mm)	$l_4 = 2x_1$ (mm)	$l_4 = 4x_1 = l_2$ (mm)	l_1 (mm)	COP_s	d_1 (mm)	W_s (W)	W_{cx} (W)	W_{ax} (W)
H ₂	400	102	102	7.2	14.4	37	2.47	311	405	98.8	76.9
	500	82	82	5.8	11.6	30	2.45	313	408	99.8	77.6
	600	68	68	4.8	9.6	25	2.43	314	412	101	78.3
He	400	39	79	4.1	8.2	51	2.75	426	364	127	119
	500	32	63	3.3	6.6	41	2.65	434	378	132	124
	600	26	53	2.8	5.6	34	2.54	443	393	138	129

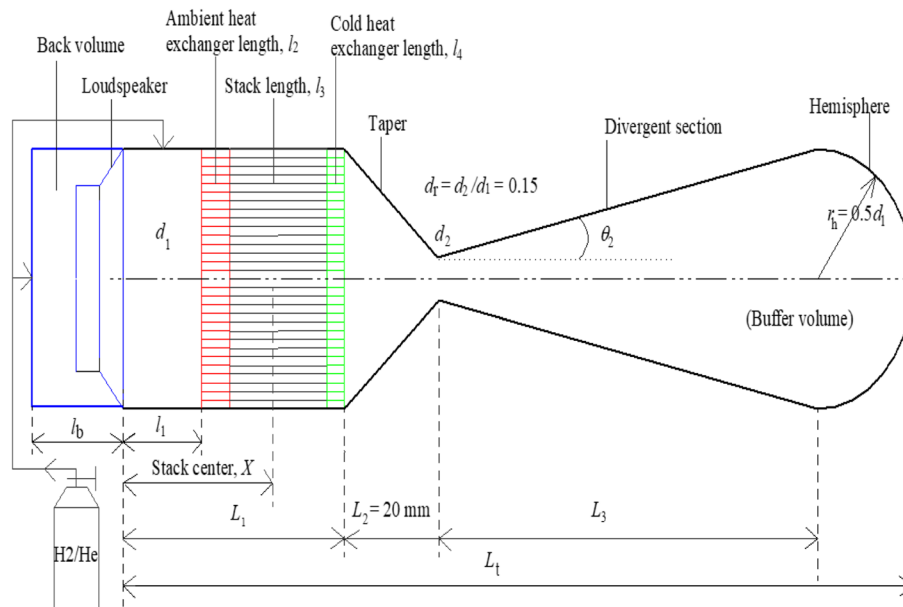


Fig. 4 A schematic representation of the resonator with taper-divergent-hemispherical design

open end for the oscillating gas where the velocity is maximum [1, 9, 26]. The stainless-steel resonator sheet with a thickness of 0.5 mm is self-sufficient to sustain the dynamic pressure amplitude of 10 bar gas pressure. The stainless-steel sheet is the best choice compared to aluminium and Delrin materials to minimise the acoustic dissipation losses and gas leakage and threading problems associated during experimentation as discussed elsewhere [2, 3]. The stainless-steel material has the following properties: thermal conductivity (k) $14.06 \text{ Wm}^{-1} \text{ K}^{-1}$, density (ρ) 7924.2 kgm^{-3} and specific heat (C_p) $445.91 \text{ Jkg}^{-1} \text{ K}^{-1}$. The speaker modified with the gas back volume (called driver) which match the speaker frequency with the resonance frequency to increase the efficiency from 3% to about 50–90% possible [6, 27–29].

The gas back volume (Fig. 4) which match the loudspeaker frequency and the resonance frequency. It is of 600 Hz for hydrogen and 400 Hz for helium. The moving coil spring constant 's' of the loudspeaker [5] is

$$s = 4\pi^2(f)^2 m \tag{16}$$

where 'm' is the mass of the vibrating material. The gas back volume for the driver [5] is

$$V_b = \frac{\gamma P A_b^2}{s} \tag{17}$$

where 'γ' is the index of compression or expansion of gas, 'P' is the oscillating gas pressure, 'A_b' is the area of cross section of back volume. In the literature it is found that the driver has maximum efficiency when the area of cross section of back volume (A_b), the vibrating diaphragm of driver (A_d) and the cross section of stack (A₁) are equal [30–34]. In Table 7 the design and electro-mechanical parameters of the speaker with gas back volume for hydrogen and helium are presented.

Substituting the data of Tables 1, 2 and 7 in Eqs. (16) and (17), the spring constant 's' and gas back volume 'V_b' and its length 'l_b' are determined for both hydrogen and helium (Table 7). The resonator full length of quarter-wavelength design 'L_t' measured from the driver surface and the hemispherical end for both the hydrogen and helium is given by

$$L_t = 0.25\lambda \tag{18}$$

For the taper-divergent-hemispherical design (Fig. 4), the angle of diverging section 'θ₂' varies inversely with its diverging length 'L₃'. Because of the better properties of hydrogen compared to helium (Tables 1, 2, 3 and 4), the

Table 7 The driver electro-mechanical parameters with hydrogen and helium

Common parameters	H ₂ parameters	He parameters
$R_e = 12 \Omega$, $L_e = 0.0039 \text{ H}$, $Bl = 75 \text{ T-m}$, $m = 75 \text{ g}$, $R_m = 9 \text{ Nsm}^{-1}$	$A_d = 774.1 \text{ cm}^2$, $V_b = 7871 \text{ cm}^3$, $l_b = 102 \text{ mm}$, s at $f_d = 600 \text{ Hz} = 1065.9 \text{ kNm}^{-1}$	$A_d = 1422.3 \text{ cm}^2$, $V_b = 72,588 \text{ cm}^3$, $l_b = 510 \text{ mm}$, s at $f_d = 400 \text{ Hz} = 473.7 \text{ kNm}^{-1}$

hydrogen at 600 Hz has the smaller length ' L_3 ' and the angle ' θ_2 ', and the smaller resonator length ' L_t ' and the volume ' V_T '. This in turn leading to 2.1 times better power-density over helium at 400 Hz (refer Table 8). Thus, the compact hydrogen resonator has only the 0.6 times the acoustic-power absorption ' W_r ' in to the internal surfaces of the resonator compared to the helium resonator (Table 8).

Using the values of Table 1 and 2 in Eq. (5) and (6) and the acoustic-power dissipation in the resonator internal surface area ' w_r ' between the driver the and ambient heat-exchanger, and in the taper-divergent-hemispherical portion of the resonator with hydrogen and helium is given by [5]

$$w_r = 0.25\rho u_1^2 \delta_v \omega + 0.25 \frac{p_1^2 (\gamma - 1) \delta_k \omega}{\rho u^2} \quad (19)$$

Hydrogen has the lower acoustic power dissipation compared to helium because of its compact design. The acoustic-power dissipation into the individual resonator component is determined by multiplying Eq. (19) with its internal surface area. The total acoustic-power input to the resonator ' W_r ' is the sum of all the individual resonator component acoustic power dissipation. Excluding the heat-exchangers (Refer Fig. 4), the stainless-steel sheet resonator and the stack length is assumed to be super insulated or placed under the vacuum vessel to avoid the heat leak losses as discussed elsewhere [1, 3, 35]. Using the values given in Tables 6 and 8, the total acoustic-power dissipation ' W_t ' into the parallel plates stack, heat-exchangers, and the resonator is given by

$$W_t = W_s + W_{cx} + W_{ax} + W_r \quad (20)$$

The heat rejection rate of the ambient heat-exchanger ' Q_r ', performance of the cooler 'COP', Carnot's 'COPC' and relative 'COPR' with hydrogen and helium for the 1 kW cooler is calculated using Eqs. (21) - (24) given below.

$$Q_r = W_t + Q \quad (21)$$

$$\text{COP} = \frac{Q}{W_t} \quad (22)$$

$$\text{COPC} = \frac{T_{cx}}{\theta} \quad (23)$$

$$\text{COPR} = \frac{\text{COP}}{\text{COPC}} \quad (24)$$

The hydrogen offers minimum acoustic resistance since it has good thermo-physical properties over helium (refer Table 1). The hydrogen resonator has the smaller heat rejection rate ' Q_r ' since it has the smaller total acoustic-power dissipation ' W_t ' in the cooler components (Table 8) compared to helium. Thus, the hydrogen cooler resulting with the better coefficient of performance and power-density over helium because of the decrease in the acoustic-power dissipation in the heat exchangers (Table 6). The low-cost hydrogen, which is about 2.5 times less expensive compared to helium. Hence hydrogen may be considered as one of the best working gasses for thermoacoustic coolers with the necessary safety precautions to avoid the danger of explosion.

4 DeltaEC results and discussion

In this section the theoretically optimized quarter wavelength taper-divergent-hemispherical design resonator (Fig. 4) with hydrogen and helium is tested in the 'Design environment for low-amplitude thermo-acoustic Energy Conversion-DeltaEC' software [13] for validation. The software anticipates the physical performance of the thermoacoustic devices (coolers and engines) using the one-dimensional (1D) computer program for linear analysis. The results are analysed by considering the assumptions, constraints and the limitations of the DeltaEC software as well as the theoretical design. The DeltaEC integrates the 1D Nikolaus Rott's governing thermoacoustic wave, heat, and acoustic-power equations of the oscillating gas for the model proposed by a designer in a computer programme [15, 22, 23]. The software uses the geometric sequential segments of the thermoacoustic cooler in a programme, namely the loudspeaker, duct, ambient heat-exchanger, stack, cold heat-exchanger, taper, cones, and the compliance. A designer develops the DeltaEC program using the statements, namely the BEGIN, Insert, Kill, Append, VESPEAKER, Duct, HX, STKSLAB, CONE, COMPLIANCE, HARDEND, etc. These segments do not have the heat leak losses with the surrounding environment since they are assumed to be insulated perfectly by default including the driver using the INSULATE statement. The driver electric power input ' E ' with

Table 8 The optimized quarter-wavelength resonator parameters for hydrogen and helium

Gas	f (Hz)	L_1 (mm)	L_3 (mm)	θ_2 (°)	L_t (mm)	V_T (L)	P_v (kW/m ³)	W_r (W)	W_t (W)	Q_r (W)	COP	COPR
H ₂	600	112	246	28.5	535	24.8	40.3	13.3	604	1604	1.65	0.239
He	400	107	279	32.9	619	52.0	19.2	22.2	632	1632	1.58	0.228

the gas back volume is equal to the sum of the acoustic-power output ' W_t ' (Eq. (20)) and its energy conversion loss. Therefore, in DeltaEC software the ambient heat-exchanger rejects heat ' Q_R ' which is equal to the sum ' E ' and ' Q ' (cooling-power) (refer Table 9). The effect of the temperature difference of the ambient and cold heat-exchangers ' θ ' at 38 K and 28 K by setting the target of 301 K for the ambient heat-exchanger and the effect of the cold heat-exchanger length ' l_4 ' equal to $2x_1$ and $4x_1$ is discussed. For both hydrogen and helium, the frequency of gas ' f ' varies inversely with the cold heat-exchanger length ' l_4 ' irrespective of the temperature difference ' θ '. The average gas temperature ' T ', mean temperature of the gas across the heat exchangers ' T_{mg} ', and mean temperature of the heat exchangers ' T_{mx} ' are presented in Table 9. It is found that the ' $T > T_{mg}$ ' and ' $T_{mg} > T_{mx}$ ' for both hydrogen and helium which is given by $T > T_{mg} > T_{mx}$.

For the temperature difference of 38 K, the DeltaEC predicts 283 K for ' T_{mg} ' and 282 K for ' T_{mx} ' at the constant ambient heat exchanger temperature of 301 K for both hydrogen and helium. It justifies the assumptions of taking the ' T_{mg} ' one kelvin greater than the ' T_{mx} ' that is $T_{mg} = (T_{mx} + 1 \text{ K})$ in the theoretical design (Table 2). The driver electric power input ' E ' and its efficiency ' η_{ea} ' is proportional to the cold heat-exchanger length ' l_4 ', and inversely proportional to the temperature difference ' θ ' for both hydrogen and helium (Table 9). This is because the increase in the length of ' l_4 ' has the higher acoustic-power absorption ' W_{cx} ' (Table 6) which in turn increases the driver electric power input ' E '. The driver efficiency ' η_{ea} ' increases as the oscillating gas offers smaller resistance on the vibrating diaphragm of the driver. Also the increase in the length of ' l_4 ' decreases the cooling power ' Q ' and the performance of the cooler (Eq. 22–24). It is because of the increase in the acoustic-power absorption in the cold heat-exchanger ' W_{cx} '. The cooling-power and performance of the cooler (Eq. 22) decreases with increase in the temperature

difference for both hydrogen and helium because of the decrease in the cold heat-exchanger temperature. But the relative coefficient of performance (Eq. 24) increases with increase in the temperature difference ' θ ' because of the decrease in the cold heat-exchanger temperature ' T_{cx} ' for both hydrogen and helium. The dynamic acoustic pressure amplitude ' P_a ' and the resonator components solid material temperature ' T_s ' as a function of the distance ' x ' measured from the driver surface along the resonator length for hydrogen and helium for the optimized TDH resonator (Fig. 4 and Table 8) is shown in Figs. 5–8.

Referring to Figs. 5 and 6, the gas dynamic acoustic pressure amplitude ' P_a ' at the driver surface where ' x ' equal to zero is found to be 0.3 bar for both hydrogen and helium, which is same as that of the theoretical design (Table 2). The gas dynamic acoustic pressure amplitude remains the same along the length of the duct (100% porosity) and decreases in the parallel plates stack and heat-exchangers system (85% porosity) for both hydrogen and helium. It decreases inordinately in the small length 20 mm taper section because of the sudden decrease in the diameter ratio of 15% (Fig. 4), and goes negative in the remaining portion of the resonator (Figs. 5 and 6). The variation of the resonator components solid material temperature ' T_s ' as a function of the distance ' x ' measured from the driver surface along the resonator length for both hydrogen and helium are shown in Figs. 7 and 8. There is a small drop in ' T_s ' along the length of the ' l_2 ' since it is targeted to a constant temperature of ' T_{ax} ' at 301 K. It decreases drastically along the stack length since it pumps heat in the stack region and remains constant in the remaining length as shown in Figs. 7 and 8.

5 Conclusion

The effect of resonance frequency of hydrogen and helium on the stack and heat-exchangers parallel plates spacing and thickness, the wavelength and the

Table 9 Simulation results of DeltaEC for the taper-divergent-hemispherical resonator design versus the working gas, temperature difference and cold heat-exchanger length

Gas	θ (K)	T_{cx} (K)	l_4 (mm)	f (Hz)	T (K)	T_{mg} (K)	T_{mx} (K)	E (W)	η_{ea} (%)	Q (W)	Q_R (W)	COP	COPR
H ₂	38	263	$2x_1 = 4.8$	559	302.8	283	282	1266	42.3	631	1897	1.28	0.184
			$4x_1 = 9.6$	557	302.8	283	282	1302	44.7	590	1892	1.11	0.160
	28	273	$2x_1 = 4.8$	569	302.9	288	287	1308	45.3	783	2091	1.41	0.145
			$4x_1 = 9.6$	567	302.9	288	287	1346	47.6	740	2086	1.24	0.128
He	38	263	$2x_1 = 4.1$	392	303.7	283	282	3359	15.9	743	4102	1.49	0.215
			$4x_1 = 8.2$	390	303.7	283	282	3405	17.4	687	4092	1.25	0.181
	28	273	$2x_1 = 4.1$	399	303.9	288	287	3413	17.8	1026	4439	1.78	0.183
			$4x_1 = 8.2$	397	303.9	288	287	3462	19.3	968	4430	1.53	0.157

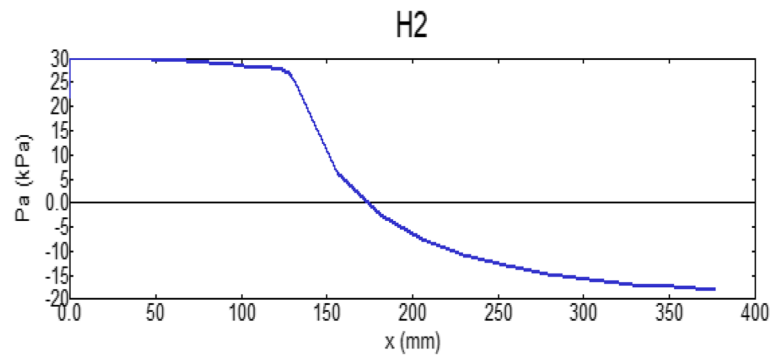


Fig. 5 Dynamic acoustic pressure amplitude of hydrogen as a function of gas position

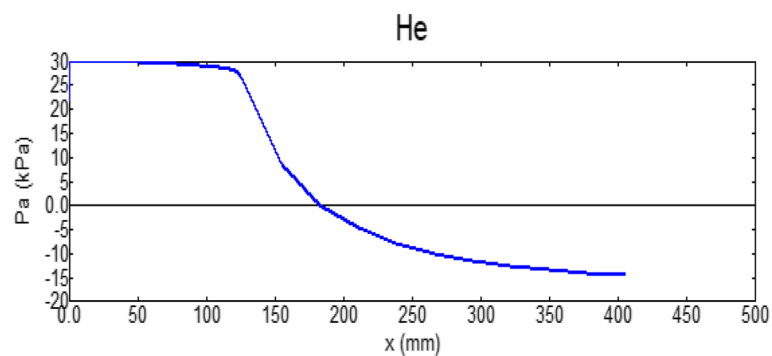


Fig. 6 Dynamic acoustic pressure amplitude of helium as a function of gas position

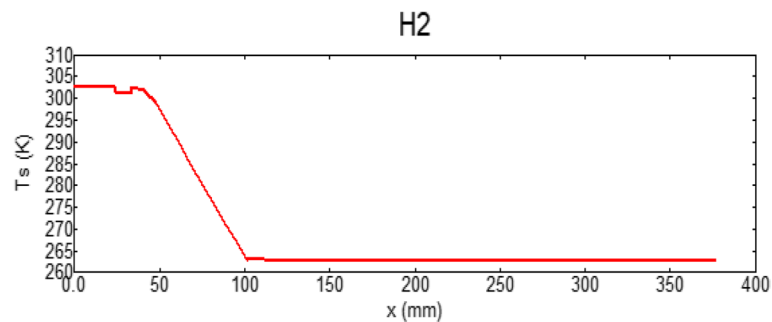


Fig. 7 Resonator solid material temperature of hydrogen as a function of gas position

performance of the stack is discussed in Sect. 2. The increase in resonance frequency decreases these four parameters (Tables 3, 4 and 6) for both the gases. It is resulting with the very thin stack-heat exchangers plate spacing and thickness (Table 3), and decrease the resonator length. The decrease in resonator length improves the power density of the cooler (Table 8). Referring to Table 6, with the increase in resonance frequency, hydrogen shows small increase in the stack diameter over helium since it has better thermo-physical properties for

a cooler (Table 1). Hence the cooler is optimized to operate with hydrogen at 600 Hz and helium at 400 Hz. The choice of operating the cooler at these two frequencies is justified based on its higher performance of the parallel plates stack and the cooler, and the power-density (Tables 6 and 8). The hydrogen shows 4.4% increase in the cooler performance and 110% increase in the power-density compared to helium.

For the taper-divergent-hemispherical resonator design (Fig. 4), the DeltaEC predicts the small decrease

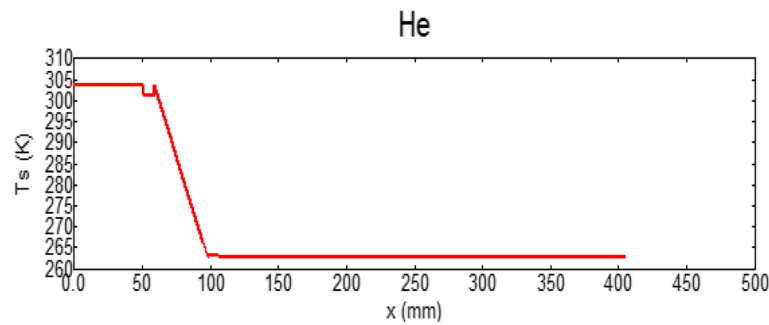


Fig. 8 Resonator solid material temperature of helium as a function of gas position

in the cooling-power (16%) and the cooler performance (13%) over helium (Table 9) with the increase in the power-density of hydrogen (Table 8). It is because of the increase in the gas turbulence with the compact design of the hydrogen cooler. Therefore, by considering the better performance, cooling-power and power-density, operating the cooler at 500 Hz for both hydrogen and helium is the best choice. Increasing the length of ' l_4 ' = ' $4x_1$ ' to facilitate the necessary space for accommodating the thermocouple [3, 35], resulting with the small decrease in the cooling power and the coefficient of performance for both hydrogen and helium (Table 9). It is because of the increase in resistance of the oscillating gas in the cold heat-exchanger length ' l_4 ' [36, 37]. The DeltaEC results show that the increase of temperature difference ' θ ' from 28 to 38 K decreases the cooling-power and coefficient of performance of the cooler for both hydrogen and helium. It is because of the increase in the acoustic resistance of the oscillating gas across the stack length ' l_3 ' while bringing down the cold heat-exchanger temperature ' T_{cx} ' from 0 °C to -10 °C.

Referring to Table 8 the theoretical cooler performance and the relative performance (Eqs. 22 and 24) are comparatively higher than the DeltaEC results (Table 9). It is because the driver parameters (Table 7) are neglected in the theoretical design. Hydrogen is less expensive compared to helium and has better thermophysical properties as a working gas (Table 1). Hydrogen is dangerous compared to helium but with the necessary safety measures, hydrogen can be used as a promising working gas for the future thermoacoustic coolers.

6 Nomenclature

Bl	Loudspeaker force factor (NA^{-1} or Tm)	He	Helium
C_p	Specific heat-isobaric ($Jkg^{-1}K^{-1}$)	H_2	Hydrogen
d_r	Diameter ratio, d_2/d_1	k	Thermal conductivity ($Wm^{-1}K^{-1}$)
E	Electric power input to loudspeaker (W)	L_1	Large diameter tube length (mm)
f	Resonance frequency (Hz)	L_e	Loudspeaker electrical inductance (H)
		l_1	Length of loudspeaker and ambient heat-exchanger (mm)
		l_2	Ambient heat-exchanger length (mm)
		l_3	Parallel plates stack length (mm)
		l_4	Cold heat-exchanger length (mm)
		m	Loudspeaker moving mass (g)
		P_v	Cooler power-density (Wm^{-3})
		Q	Cooler cooling-power (W)
		Q_r	Heat rejection by ambient heat-exchanger without gas back volume (W)
		Q_R	Total heat rejection by ambient heat-exchanger with gas back volume (W)
		R_m	Driver mechanical resistance (Nsm^{-1})
		R_e	Driver electrical resistance (Ω)
		s	Spring stiffness of driver (Nm^{-1})
		T	Average gas temperature (K)
		TDH	Taper-divergent-hemispherical resonator
		T_{cx}	Cold heat-exchanger temperature (K)
		T_{ax}	Ambient heat-exchanger temperature (K)
		T_{mg}	Gas mean temperature between heat-exchangers, K
		T_{mx}	Heat-exchangers mean temperature (K)
		u	Linear velocity of gas oscillation (ms^{-1})
		V_T	Resonator total volume (L)
		X	Centre point of parallel plates stack (mm)
		X_2	Centre point of ambient heat-exchanger (mm)
		X_4	Centre point of cold heat-exchanger (mm)
		γ	Specific heats ratio
		ρ	Material density (kgm^{-3})
		σ	Gas Prandtl number
		μ	Dynamic viscosity of gas ($kgm^{-1}s^{-1}$)
		θ_n	Normalized temperature difference of heat exchangers
		θ_2	Angle in the diverging buffer section (degrees)

Acknowledgements

This work was supported by JSSMVP Mysuru, Principal, HOD (Mechanical), and all the staff of the Department of Mechanical Engineering and JSSATE Bengaluru. Authors thank Bill Ward, John Clark, and Greg Swift, Los Alamos National Laboratory, USA for developing DeltaEC software and making it freely available for research purpose.

Authors' contributions

The author(s) read and approved the final manuscript.

Availability of data and materials

All data generated or analysed during this study are included in this article.

Declarations

Competing interests

The authors declare that they have no competing interests.

Received: 31 May 2023 Accepted: 28 August 2023

Published online: 20 September 2023

References

- Hofler, T. J. (1986). *Thermoacoustic refrigerator design and Performance*. Ph.D. dissertation, University of California, San Diego.
- Tijani, M. E. H., Zeegers, J. C. H., & de Waele, A. T. A. M. (2002). Construction and performance of a thermoacoustic refrigerator. *Cryogenics*, 42, 59–66.
- Prashantha, B. G., Govinde Gowda, M. S., Seetharamu, S., & Narasimham, G. S. V. L. (2017). Design construction and performance of 10 W thermoacoustic refrigerators. *International Journal of Air-Conditioning and Refrigeration*, 25(3), 1750023. <https://doi.org/10.1142/S2010132517500237>. 14 pages.
- Prashantha, B. G., Narasimham, G. S. V. L., Seetharamu, S., & Hemadri, V. B. (2022). Theoretical evaluation of stack-based thermoacoustic refrigerators. *International Journal of Air-Conditioning and Refrigeration*, 30, 8. <https://doi.org/10.1007/s44189-022-00008-2>
- Tijani, M. E. H. (2001). *Loudspeaker-driven thermo-acoustic refrigeration*. Ph.D. Thesis, Eindhoven University of Technology.
- Wetzel, M., & Herman, C. (1997). Design optimization of thermoacoustic refrigerator. *International Journal of Refrigeration*, 20(1), 3–21.
- Babaei, H., & Siddiqui, K. (2008). Design and optimization of thermoacoustic devices. *Energy Conversion and Management*, 49, 3585–3598.
- Prashantha, B. G., Narasimham, G. S. V. L., Seetharamu, S., & Manjunatha, K. (2021). Effect of gas blockage on the theoretical performance of thermoacoustic refrigerators. *International Journal of Air-Conditioning and Refrigeration*, 29(3), 2150026. <https://doi.org/10.1142/S2010132521500267>. 16 pages.
- Swift, G. W. (1988). Thermoacoustic engines. *Journal of the Acoustical Society of America*, 84(4), 1145–1180.
- Prashantha, B. G., Swamy, D. R., Soargaon, B., & Nanjundeswaraswamy, T. S. (2020). Design optimization and analysis of thermoacoustic refrigerators. *International Journal of Air-Conditioning and Refrigeration*, 28(3), 2050020. <https://doi.org/10.1142/S2010132520500200>. 12 pages.
- Prashantha, B. G., Govinde Gowda, M. S., Seetharamu, S., & Narasimham, G. S. V. L. (2013). Theoretical evaluation of loudspeaker for a 10-W cooling power thermoacoustic refrigerator. *International Journal of Air-Conditioning and Refrigeration*, 21(4), 1350027. <https://doi.org/10.1142/S2010132513500272>. 8 pages.
- Tijani, M. E. H., Zeegers, J. C. H., & de Waele, A. T. A. M. (2002). Prandtl number and thermoacoustic refrigerators. *Journal of the Acoustical Society of America*, 112(1), 134–143.
- Ward B, Clark J, Swift GW. Design environment for low-amplitude thermoacoustic energy conversion (DeltaEC software). Version 6.4b2.9 Los Alamos National Laboratory; 2008. Available at <http://www.lanl.gov/thermoacoustics>.
- Poese, M. E., & Garrett, S. L. (2000). Performance measurements on a thermoacoustic refrigerator driven at high amplitudes. *Journal of the Acoustical Society of America*, 107(5), 2480–2486.
- Swift, G. W. (2002). Thermoacoustics: A unifying perspective of some engines and refrigerators. *Acoustical Society of America*, 113, 5.
- Wheatley, J. C., Hofler, T., Swift, G. W., & Migliori, A. (1985). Understanding some simple phenomena in thermoacoustics with applications to acoustical heat engines. *American Journal of Physics*, 53, 147–162.
- Prashantha, B. G., Seetharamu, S., Narasimham, G. S. V. L., & Praveen Kumar, M. R. (2019). Effect of stack spacing on the performance of thermoacoustic refrigerators using helium and air as working substances. *International Journal of Air-Conditioning and Refrigeration*, 27(2), 1950016. <https://doi.org/10.1142/S2010132519500160>. 11 pages.
- Prashantha, B. G., Govinde Gowda, M. S., Seetharamu, S., & Narasimham, G. S. V. L. (2016). Design analysis of thermoacoustic refrigerator using air and helium as working substances. *International Journal of Thermal and Environmental Engineering*, 13(2), 113–120. <https://doi.org/10.5383/ijtee.13.02.006>
- Swift, G. W. (1997). Thermoacoustic engines and refrigerators. *Encyclopedia Applied Phys*, 21, 245–264.
- Narasimham, G. S. V. L., & Krishna Murthy, M. V. (1997). *Thermoacoustic Refrigeration: An Overview*. Workshop on Cryocooler Technology-Emerging Trends, Applications and Curriculum Development. Central Cryogenic Facility, IISc Bengaluru.
- Prashantha, B. G., Govinde Gowda, M. S., Seetharamu, S., & Narasimham, G. S. V. L. (2018). Design and analysis of acoustically-driven 50 W thermoacoustic refrigerators. *Sādhanā*, 43, 82. <https://doi.org/10.1007/s12046-018-0860-8>
- Rott, N. (1969). Damped and thermally driven acoustic oscillations in wide and narrow tubes. *Zeitschrift für Angewandte Mathematik und Physik*, 20, 230–243.
- Rott, N. (1980). Thermoacoustics. *Advances in Applied Mechanics*, 20, 135–175.
- Prashantha, B. G., Govinde Gowda, M. S., Seetharamu, S., & Narasimham, G. S. V. L. (2013). Design and analysis of thermoacoustic refrigerator. *International Journal of Air-Conditioning and Refrigeration*, 21(1), 1350001. <https://doi.org/10.1142/S2010132513500016>. 10 pages.
- Prashantha, B. G., Govinde Gowda, M. S., Seetharamu, S., & Narasimham, G. S. V. L. (2017). Design and comparative analysis of thermoacoustic refrigerators. *International Journal of Air-Conditioning and Refrigeration*, 25(1), 1750002. <https://doi.org/10.1142/S201013251750002X>. 9 pages.
- Prashantha, B. G., Govinde Gowda, M. S., Seetharamu, S., & Narasimham, G. S. V. L. (2015). Resonator optimization and studying the effect of drive ratio on the theoretical performance of a 10-W cooling power thermoacoustic refrigerator. *International Journal of Air-Conditioning and Refrigeration*, 23(3), 1550020. <https://doi.org/10.1142/S2010132515500200>. 12 pages.
- Wakeland, R. S. (2000). Use of electrodynamic drivers in thermoacoustic refrigerators. *Journal of the Acoustical Society of America*, 107, 827–832.
- Garrett, S. L., Adeff, J. A., & Hofler, T. J. (1993). Thermoacoustic refrigerator for space applications. *Journal of Thermophysics and Heat Transfer*, 7, 595–599.
- Prashantha, B. G., Govinde Gowda, M. S., Seetharamu, S., & Narasimham, G. S. V. L. (2014). Design and optimization of a loudspeaker-driven 10 W cooling power thermoacoustic refrigerator. *International Journal of Air-Conditioning and Refrigeration*, 22(3), 1450015. <https://doi.org/10.1142/S2010132514500151>. 15 pages.
- Prashantha, B. G., Seetharamu, S., Narasimham, G. S. V. L., & Praveen Kumar, M. R. (2019). Design and analysis of thermoacoustic refrigerators using air as working substance. *International Journal of Air-Conditioning and Refrigeration*, 27(1), 1950008. <https://doi.org/10.1142/S2010132519500081>. 14 pages.
- Zolpakar, N. A., Mohd-Ghazali, N., & El-Fawal, M. H. (2016). Performance analysis of the standing wave thermoacoustic refrigerator: A review. *Renewable and Sustainable Energy Reviews*, 54, 626–34. <https://doi.org/10.1016/j.rser.2015.10.018>
- Prashantha, B. G., Govinde Gowda, M. S., Seetharamu, S., & Narasimham, G. S. V. L. (2013). Theoretical evaluation of 10-W cooling power thermoacoustic refrigerator. *Heat Transfer-Asian Research*, 43(7), 557–91. <https://doi.org/10.1002/htj.21094>
- Tijani, M. E. H., Zeegers, J. C. H., & de Waele, A. T. A. M. (2002). A gas-spring system for optimizing loudspeakers in thermoacoustic refrigerators. *Journal of Applied Physics*, 92(4), 2159–2165.

34. Akhavanbazaz, M., Kamran Siddiqui, M. H., & Bhat, R. B. (2007). The impact of gas blockage on the performance of a thermoacoustic refrigerator. *Experimental Thermal and Fluid Science*, 32, 231–9. <https://doi.org/10.1016/j.expthermflusci.2007.03.009>
35. Tijani, M. E. H., Zeegers, J. C. H., & de Waele, A. T. A. M. (2002). The optimal stack spacing for thermoacoustic refrigeration. *Journal of the Acoustical Society of America*, 112(1), 128–133.
36. Prashantha, B. G., Seetharamu, S., Narasimham, G. S. V. L., & Manjunatha, K. (2023). Effect of gas spacing and resonance frequency on theoretical performance of thermoacoustic refrigerators. *International Journal of Air-Conditioning and Refrigeration*, 31, 11. <https://doi.org/10.1007/s44189-023-00027-7>
37. Kamil, M. Q., Yahya, S. G., & Azzawi, I. D. J. (2023). Design methodology of standing-wave thermoacoustic refrigerator: Theoretical analysis. *International Journal of Air-Conditioning and Refrigeration*, 31, 7. <https://doi.org/10.1007/s44189-023-00023-x>

Publisher's Note

Springer Nature remains neutral with regard to jurisdictional claims in published maps and institutional affiliations.